Smart Dust Option for Geomagnetic Tail Exploration

Alessandro A. Quarta*, Giovanni Mengali, Lorenzo Niccolai

Department of Civil and Industrial Engineering, University of Pisa, I-56122 Pisa, Italy

Abstract

In-situ measurements are necessary for a long-term analysis of the spatial structure of the geomagnetic tail. This type of long length mission requires the use of a propellantless propulsion system, such as a classical solar sail, to continuously rotate the design orbit apse line such that it remains parallel to the Sun-Earth direction. To reduce the mission costs, this paper suggests the employment of Sun-pointing smart dusts, which are here investigated in terms of propulsive acceleration level necessary to guarantee a mission feasibility. A Sun-pointing smart dust can be thought of as a millimeter-scale solar sail, whose geometric configuration allows it to passively maintain an alignment with the Sun-spacecraft line. The smart dust external surface is coated with an electrochromic reflective film in such a way that it may change, within some limits, its propulsive acceleration magnitude. A suitable control law is necessary for the smart dust to enable an artificial precession of its Earth-centred orbit, similar to what happens in the GeoSail mission. This paper analyzes the required control law using an optimal approach. In particular, the proposed mathematical model provides a set of approximate equations that allow a simple and effective tradeoff analysis between the propulsive requirements, in terms of the smart dust acceleration, and the characteristics of the design orbit.

Keywords: smart dust, femto solar sail, electrochromic control system, geomagnetic tail exploration

Nomenclature

a	osculating orbit semimajor axis (km)
$\boldsymbol{a}_p$	propulsive acceleration, with $a_p \triangleq \|\boldsymbol{a}_p\|$ (mm/s^2)
a_{p_r}	radial component of $\boldsymbol{a}_p$ (mm/s^2)
a_{p_t}	transverse component of $\boldsymbol{a}_p$ (mm/s^2)
$a^\star_{p_{\min}}$	reference value; see Eq. (21) (mm/s^2)
A/m	area-to-mass ratio (m^2/kg)
e	osculating orbit eccentricity
$E^\star$	eccentric anomaly when $r = r^\star$ (deg)
f	dimensionless auxiliary function; see Eq. (31)
F	dimensionless auxiliary function; see Eq. (34)
G	dimensionless auxiliary function; see Eq. (35)
$\mathcal{H}$	Hamiltonian function
$\hat{\boldsymbol{i}}$	orbital reference frame unit vector

*Corresponding author

Email addresses: a.quarta@ing.unipi.it (Alessandro A. Quarta), g.mengali@ing.unipi.it (Giovanni Mengali), lorenzo.niccolai@ing.unipi.it (Lorenzo Niccolai)

Published in Astrodynamics, Vol. 3, September 2019, pp. 217–230. doi: https://doi.org/10.1007/s42064-019-0048-3

J	performance index
n	design parameter
O	Earth's center-of-mass
p	osculating orbit semilatus rectum (km)
r	Earth-SPSD distance (km)
$r^\star$	reference distance (km)
$\hat{\boldsymbol{r}}_\odot$	Sun-SPSD unit vector
$R_\oplus$	Earth's mean radius (km)
S_W	switching function; see Eq. (19)
t	time (days)
$\mathcal{T}(O; \hat{\boldsymbol{i}}_r, \hat{\boldsymbol{i}}_t)$	orbital reference frame
δ	Earth-Sun line angle (deg)
Δt_{sp}	scientific phase time interval (days)
λ_i	variables adjoint to ith state
$\mu_\oplus$	Earth's gravitational parameter (km^3/s^2)
ν	osculating orbit true anomaly (deg)
$\nu^\star$	true anomaly when $r = r^\star$ (deg)
ϕ	auxiliary angle; see Eq. (7) (deg)
τ	dimensionless switching parameter
ω	osculating orbit argument of perigee (deg)
$\Omega_\oplus$	Earth's orbital angular velocity (deg/day)

Subscripts

0	initial
a	apogee
ac	constrained to $a_{p_{\min}}$
f	final
max	maximum
min	minimum
p	perigee
r	radial
t	transverse

Superscripts

max	maximum
min	minimum
$\wedge$	unit vector

1. Introduction

An in-depth knowledge of the complex physical phenomena that govern the plasma dynamics within the Earth's magnetosphere, especially in the magnetotail region, is known to have a great importance from both a scientific and a technical viewpoint. For example, the availability of accurate models is a necessary prerequisite for a successful forecasting capability of the space weather, including the ability to anticipate an imminent storm and protect orbiting spacecraft as well as electrical systems on the ground. Since the dynamical models developed for Earth are expected to be valid in the magnetospheres of the other terrestrial planets, their study is extremely useful for improving our knowledge of planets' internal structure and hence for better understanding the intrinsic properties of our planetary system [1].

To solve the above problems, *in-situ* measurements are necessary. A long-term residence of a spacecraft in the geomagnetic tail allows important scientific objectives, such as the occurrence of magnetic reconnection or the magnetospheric boundary layer, to be investigated. This mission scenario requires the payload to be placed into an elliptic orbit with a high apogee radius to explore the whole geomagnetic tail. Unfortunately, a conventional Keplerian orbit, with its fixed orientation in space, is not of practical use, because the geomagnetic tail is always aligned along the Sun-Earth line and, as such, it rotates with respect to an inertial (heliocentric) reference frame. This implies that the apse line of a Keplerian orbit would be aligned with the geomagnetic tail once per year only. As a result, considering the geomagnetic tail dimensions, about 3 months of data could be acquired, with only 1 month of accurate data from the tail axis [2]. To guarantee a continuous flux of *in-situ* measurements, the apse line of the spacecraft orbit is required to artificially precess at an angular rate equal to that of the Earth in its heliocentric orbit, equal to about $0.9856\,\mathrm{deg/day}$. However, previous studies [3] have shown that the ΔV required to precess such orbit by chemical (or electric) propulsion is very large, on the order of $3.5\,\mathrm{km/s}$ (or $4.5\,\mathrm{km/s}$) per year, making conventional thrusters unable to guarantee a sufficiently long mission length, due to propellant mass constraints.

A possible solution, which guarantees long stay times in the Earth's magnetotail, is offered by the GeoSail mission concept [2, 3, 4, 5]; see Fig. 1. In that mission, the required Sun-synchronous apse-line precession is obtained by means of a classical solar sail, thus avoiding the conventional limits imposed by propellant consumption. Assuming an ideal force model [6], McInnes et al. [3] have proposed a simple steering law that consists in orienting the sail nominal plane such that its normal is always directed along the Sun-spacecraft line. A more effective control law is discussed in Ref. [7] from an optimal viewpoint.

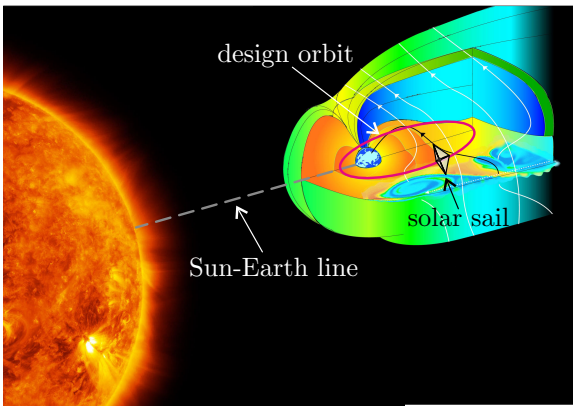

Figure 1: GeoSail mission concept for geomagnetic exploration; courtesy of Dr. Hiroshi Hasegawa.

The concept described in this paper is similar to that proposed in the GeoSail mission, but now the artificial precession of the apse line is obtained by means of smart dusts (SDs). A SD is a femtosatellite with a maximum side length of a few centimeters and a high area-to-mass ratio [8, 9, 10, 11]. The latter characteristic allows the SD to exploit the solar radiation pressure as a propulsive force in a similar way as a solar sail does [12]. Actually, a SD is essentially a micro solar sail spacecraft with all of the subsystems integrated on a single plate [13]. With suitable strategies, such as the use of facets, the SD may be designed such as to passively maintain a Sun-facing attitude. The latter configuration will be therefore referred to as

Sun Pointing Smart Dust (SPSD). Its thrust level can be changed by means of an Electrochromic Control System (ECS), which uses electrochromic material coated on the SD external surface [14, 15]. The optical properties of electrochromic materials change when a suitable voltage is applied. In particular, when an ECS is activated, the SPSD specular reflection coefficient increases, thus increasing the generated thrust for a fixed area-to-mass ratio. In fact, assuming that the optical properties of the electrochromic material may be changed between two states, the SPSD thrust will vary between two different values, the larger (smaller) of which corresponds to when the ECS state is activated (deactivated). With this strategy, its dynamics may be simply but effectively controlled. The main advantage of SDs over conventional spacecraft is in their much smaller sizes and costs, to such an extent that a number of them can be stored within a single mother spacecraft and then released in the desired orbit [16]. An important shortcoming is their reduced communication capability. However, although a direct link with Earth could be impossible at current technology level, each SD could communicate with the mother spacecraft which, in turn, would be responsible of collecting the scientific data and transmit them to the ground station. Also, using multiple SPSDs, the whole geomagnetic tail could be filled with sensors that precess with the same rate as the geomagnetic tail, thus enabling a real-time 3-D visualization of the plasma structure in the magnetosphere.

Considering a SPSD with an electrochromic material coated on its surface, the question arises on whether its propulsive acceleration may be sufficient for a GeoSail-like mission. This problem is addressed in this paper from an optimal viewpoint, by looking for the minimum propulsive acceleration necessary for the SPSD to precess the apse line of the reference orbit at a Sun-synchronous angular rate. It is shown that its solution is consistent with the current technology level. A semi-analytical model is also discussed, which may be effectively used for analyzing the tradeoff performance between the required acceleration level and the length of the scientific phase per orbital revolution.

2. Mission analysis

Consider a SPSD in an elliptical Earth-centred orbit of semimajor axis a_0 and eccentricity e_0, whose orbital plane coincides with the ecliptic plane. Introduce a two-dimensional radial-tangential reference frame $\mathcal{T}(O; \hat{\boldsymbol{i}}_r, \hat{\boldsymbol{i}}_t)$, in which the origin coincides with the Earth's center-of-mass O, $\hat{\boldsymbol{i}}_r$ is the radial unit vector along the O-SPSD line, and $\hat{\boldsymbol{i}}_t$ is the transverse unit vector directed in the sense of the SPSD motion; see Fig. 2.

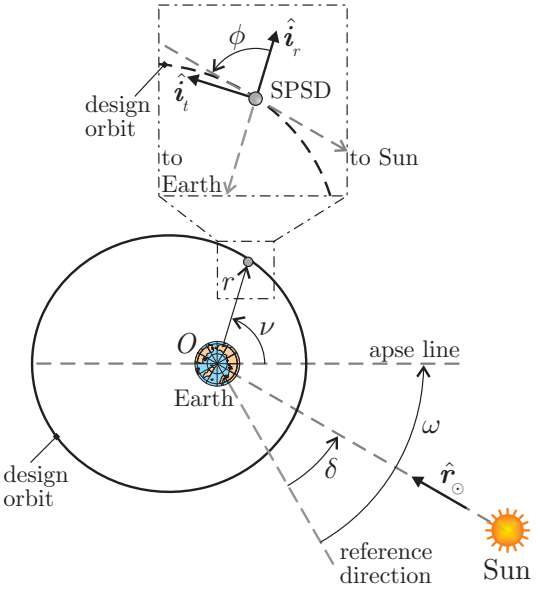

Figure 2: Reference frame and design orbit conceptual scheme.

Using the mathematical model discussed by McInnes et al. [3], the two-dimensional motion of the SPSD

may be described by the following Lagrange's planetary equations in Gaussian form [17]

$$\frac{\mathrm{d}a}{\mathrm{d}\nu} = \frac{2\,p\,r^2}{\mu_\oplus\,(1-e^2)^2}\left[a_{p_r}\,e\,\sin\nu + \frac{a_{p_t}\,p}{r}\right] \tag{1}$$

$$\frac{\mathrm{d}e}{\mathrm{d}\nu} = \frac{r^2}{\mu_\oplus}\left[a_{p_r}\,\sin\nu + a_{p_t}\left(\cos\nu + \frac{r\,\cos\nu + e\,r}{p}\right)\right] \tag{2}$$

$$\frac{\mathrm{d}\omega}{\mathrm{d}\nu} = \frac{r^2}{\mu_\oplus\,e}\left[-a_{p_r}\,\cos\nu + a_{p_t}\,\sin\nu\left(1+\frac{r}{p}\right)\right] \tag{3}$$

$$\frac{\mathrm{d}t}{\mathrm{d}\nu} = \frac{r^2}{\sqrt{\mu_\oplus\,p}}\left\{1 - \frac{r^2}{\mu_\oplus\,e}\left[a_{p_r}\,\cos\nu - a_{p_t}\,\sin\nu\left(1+\frac{r}{p}\right)\right]\right\} \tag{4}$$

where $\mu_\oplus$ is the Earth's gravitational parameter, t is the time, r is the O-SPSD distance, while, with reference to the osculating orbit parameters, ν is the true anomaly, a is the semimajor axis, ω is the argument of perigee measured counterclockwise from a reference (fixed) direction, see Fig. 2, and p is the semilatus rectum, with

$$p = a\,\left(1-e^2\right) \qquad , \qquad r = \frac{p}{1+e\,\cos\nu} \tag{5}$$

In Eqs. (1)–(4), $a_{p_r} \triangleq \boldsymbol{a}_p \cdot \hat{\boldsymbol{\imath}}_r$ (or $a_{p_t} \triangleq \boldsymbol{a}_p \cdot \hat{\boldsymbol{\imath}}_t$) is the component of the propulsive acceleration vector $\boldsymbol{a}_p$ along (or perpendicular to) the O-SPSD direction; see Fig. 2. Note that the dynamics model described by Eqs. (1)–(4) assumes the perturbing effects due to Earth's oblateness and lunisolar gravitational attractions to be negligible compared to the propulsive acceleration of the SPSD induced by the solar radiation pressure [3].

The propulsive acceleration components $\{a_{p_r},\, a_{p_t}\}$ can be written as a function of the SPSD design characteristics and the osculating orbit parameters, as is described in the next section.

2.1. Sun-pointing smart dust thrust model

The propulsive acceleration vector of an Earth-orbiting SPSD with an active ECS is obtained by suitably adapting the mathematical model discussed in Refs. [18, 19, 20], which describes the SPSD motion in a heliocentric two-dimensional case. To this end, let $a_{p_{\max}}$ (or $a_{p_{\min}}$) be the maximum (or minimum) value of $a_p \triangleq \|\boldsymbol{a}_p\|$, obtained when the ECS is switched on (or off); see Fig. 3.

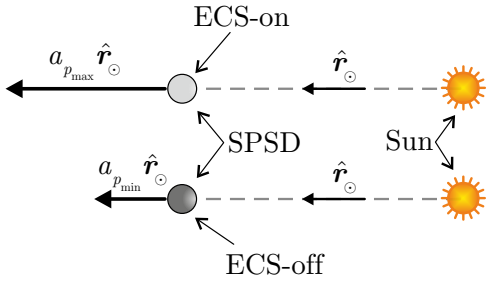

Figure 3: Conceptual scheme of a SPSD.

To a first order, the Sun-SPSD distance is nearly constant and equal to $r_\oplus \triangleq 1\,\mathrm{au}$, while the Sun-SPSD unit vector roughly coincides with the Sun-Earth unit vector $\hat{\boldsymbol{r}}_\odot$; see Fig. 2. These assumptions amount to neglecting the Earth's orbit eccentricity and the Earth-SPSD distance r with respect to the Earth-Sun distance $r_\oplus$. Note that, according to Fig. 2, the Sun-SPSD unit vector can be written as

$$\hat{\boldsymbol{r}}_\odot = \cos\phi\,\hat{\boldsymbol{\imath}}_r + \sin\phi\,\hat{\boldsymbol{\imath}}_t \tag{6}$$

in which ϕ is an auxiliary angle defined as

$$\phi \triangleq \pi - \nu + \delta - \omega \tag{7}$$

where $\delta \in [0,\, 2\,\pi]$ rad is the angle between the reference direction and the O-Sun line. Without loss of generality, assume $\delta = 0$ at the initial time $t = t_0 \triangleq 0$, that is, the apse line of the SPSD osculating orbit is initially aligned with the Earth-Sun line. Accordingly, the time variation of δ can be written as

$$\delta = \Omega_{\oplus}\, t \tag{8}$$

where $\Omega_{\oplus} \triangleq 0.9856$ deg/day is the Earth's orbital angular velocity, in accordance with the assumption of constant Earth-Sun distance (equal to $r_{\oplus}$).

Since the Sun-pointing condition requires the direction of $\boldsymbol{a}_p$ to coincide with the Sun-SPSD line, the propulsive acceleration vector may be written as

$$\boldsymbol{a}_p = a_{p_{\min}}\, [1 + \tau\,(n-1)]\, \hat{\boldsymbol{r}}_{\odot} \tag{9}$$

where $\tau \in \{0,\, 1\}$ is a time-varying (switching) control parameter that models the on/off behavior of the ECS [20], while $n \triangleq (a_{p_{\max}}/a_{p_{\min}}) \in [1,\, 2]$ is a design parameter whose value only depends on the thermo-optical characteristics of the electrochromic reflective film [15, 11]. The interval extremes within which n ranges, correspond to a fully absorptive ($n = 1$) or a specular reflecting ($n = 2$) electrochromic film. In particular, a value of $n = 1.8$ is consistent with a case [18] in which all of the impinging photons are absorbed when the ECS is switched-off, and a non-specular (incomplete) reflection [21, 22] when the ECS is switched-on. Note that $a_{p_{\min}}$ in Eq. (9) also depends on the SPSD area-to-mass ratio A/m, that is, the ratio of the effective illuminated surface (i.e., the area projected along $\hat{\boldsymbol{r}}_{\odot}$) to the smart dust total mass. Assuming $n = 1.8$ and using the results of Refs. [8, 20], Tab. 1 summarizes the values of $\{A/m,\, a_{p_{\min}},\, a_{p_{\max}}\}$ for a low- (SPSD_1), medium- (SPSD_2), and high-performance (SPSD_3) configuration.

Table 1: Values of $\{A/m,\, a_{p_{\min}},\, a_{p_{\max}}\}$ for a low- (SPSD_1), medium- (SPSD_2), and high-performance (SPSD_3) smart dust with $n = 1.8$. Data adapted from Refs. [8, 20]

	SPSD_1	SPSD_2	SPSD_3
$A/m\,[\text{m}^2/\text{kg}]$	17.39	32.61	54.63
$a_{p_{\min}}\,[\text{mm/s}^2]$	0.0794	0.1487	0.2491
$a_{p_{\max}}\,[\text{mm/s}^2]$	0.1429	0.2676	0.4483

Substituting Eqs. (6)–(8) into Eq. (9) it is found that

$$a_{p_r} = -a_{p_{\min}}\, [1 + \tau\,(n-1)]\, \cos\left(\nu + \omega - \Omega_{\oplus}\, t\right) \tag{10}$$

$$a_{p_t} = a_{p_{\min}}\, [1 + \tau\,(n-1)]\, \sin\left(\nu + \omega - \Omega_{\oplus}\, t\right) \tag{11}$$

Note that Eqs. (10)–(11) (and so Eq. (9)) neglect the shadowing effects due to the eclipse periods, when the propulsive acceleration vanishes (or reduces) due to the Earth's shadow cone. In fact, Ref. [7] shows that the eclipse periods have a negligible effect on the optimal steering law of a solar sail-based mission for the geomagnetic tail exploration.

2.2. Problem description and trajectory optimization

A continuous analysis of the spatial structure of the geomagnetic tail through *in-situ* measurements [3, 23] requires a space vehicle to cover a highly elliptic orbit, of which the apse line should precess at a rate equal to $\Omega_{\oplus}$; see Fig. 4.

According to the results of Ref. [2], the design orbit perigee is located on the Earth's dayside at a radius $r_p = 11\, R_{\oplus}$ (where $R_{\oplus}$ is the Earth's reference radius), while the apogee is aligned with the geomagnetic tail on the Earth's nightside at a radius $r_a \in [22,\, 30]\, R_{\oplus}$. Although communications with Earth at these altitudes could be difficult for a femtosatellite at current technology level, one or more smart dusts could be

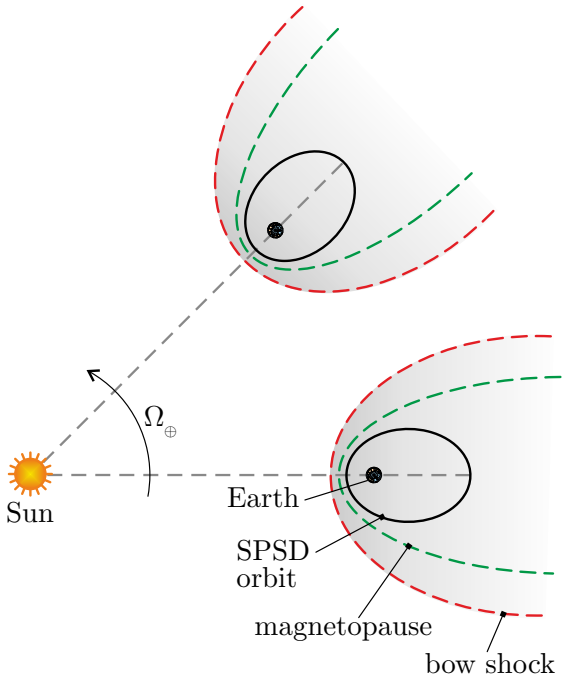

Figure 4: Conceptual sketch of artificial apse line precession.

released by a mother spacecraft [16], which could collect the scientific data and transmit them to the ground station. Such a feature is able to increase the mission lifetime and its flexibility, since a set of smart dusts could accomplish different scientific observations. In this context, with reference to the mission scenario analyzed in Refs. [2, 4, 7], in the remainder of this work a nominal value of $r_a = 23\,R_\oplus$ will be assumed, such that the value of the design orbit semimajor axis is $a_0 = 17\,R_\oplus$, whereas the design eccentricity is $e_0 = 12/34 \simeq 0.353$. Assuming, without loss of generality, that $\nu(t_0) = \nu_0 \triangleq 0$ and $\omega(t_0) = 0$ (that is, the SPSD is initially at the perigee, and the apse line is aligned with the Earth-Sun direction), the differential system of Eqs. (1)–(4) is completed by the initial conditions

$$a(\nu_0) = a_0 \equiv 17\,R_\oplus \quad , \quad e(\nu_0) = e_0 \equiv 12/34 \quad , \quad \omega(\nu_0) = 0 \quad , \quad t(\nu_0) = 0 \tag{12}$$

The time-variation (or, equivalently, the ν-variation, that is, the variation with respect to the true anomaly $\nu \in [0,\, 2\pi]\,\mathrm{rad}$) of the switching parameter τ, which allows the apse line to precess at the desired rate $\Omega_\oplus$, can be obtained as the solution of an optimal control problem, in which the performance index

$$J \triangleq -a_{p_{\min}} \tag{13}$$

is to be maximized as a function of $\tau = \tau(\nu)$, with the terminal constraints

$$a(\nu_f) = a_0 \quad , \quad e(\nu_f) = e_0 \quad , \quad \omega(\nu_f) = \Omega_\oplus\, t_f \tag{14}$$

where t_f is the time at which $\nu = \nu_f \triangleq 2\,\pi\,\mathrm{rad}$. The solution to this problem is the value of $a_{p_{\min}}^{(\min)} \triangleq \min\{a_{p_{\min}}\}$, that is, the minimum propulsive acceleration magnitude necessary for the SPSD to align the apse line of the reference orbit with the Earth-Sun direction, when the SPSD completes a single revolution around the Earth; see Eqs. (14).

To look for a solution of the optimal problem, an auxiliary differential equation is first added to the Lagrange's planetary equations, that is

$$\frac{\mathrm{d}a_{p_{\min}}}{\mathrm{d}\nu} = 0 \tag{15}$$

which simply states that $a_{p_{\min}}$, once selected, is a constant of motion. The optimal control problem is solved using an indirect method, in which the Hamiltonian function $\mathcal{H}$ is defined as [24, 25]

$$\mathcal{H} \triangleq \lambda_a \frac{\mathrm{d}a}{\mathrm{d}\nu} + \lambda_e \frac{\mathrm{d}e}{\mathrm{d}\nu} + \lambda_\omega \frac{\mathrm{d}\omega}{\mathrm{d}\nu} + \lambda_t \frac{\mathrm{d}t}{\mathrm{d}\nu} + \lambda_{ap} \frac{\mathrm{d}a_{p_{\min}}}{\mathrm{d}\nu} \tag{16}$$

where $\{\lambda_a,\, \lambda_e,\, \lambda_\omega,\, \lambda_t,\, \lambda_{ap}\}$ is the set of variables adjoint to the states $\{a,\, e,\, \omega,\, t,\, a_{p_{\min}}\}$. Using Eqs. (1)–(4) and (15) the Hamiltonian function becomes

$$\mathcal{H} = \frac{2\,p\,r^2\,\lambda_a}{\mu_\oplus\,(1-e^2)^2}\,\left[a_{p_r}\,e\,\sin\nu + \frac{a_{p_t}\,p}{r}\right] + \frac{r^2\,\lambda_e}{\mu_\oplus}\,\left[a_{p_r}\,\sin\nu + a_{p_t}\,\left(\cos\nu + \frac{r\,\cos\nu + e\,r}{p}\right)\right] +$$

$$\frac{r^2\,\lambda_\omega}{\mu_\oplus\,e}\,\left[-a_{p_r}\,\cos\nu + a_{p_t}\,\sin\nu\left(1+\frac{r}{p}\right)\right] + \frac{r^2\,\lambda_t}{\sqrt{\mu_\oplus\,p}}\,\left\{1 - \frac{r^2}{\mu_\oplus\,e}\,\left[a_{p_r}\,\cos\nu - a_{p_t}\,\sin\nu\,\left(1+\frac{r}{p}\right)\right]\right\} \tag{17}$$

The ν-variation of each adjoint variable is given by the Euler-Lagrange equations [24, 25], viz.

$$\frac{\mathrm{d}\lambda_a}{\mathrm{d}\nu} = -\frac{\partial\mathcal{H}}{\partial a} \quad , \quad \frac{\mathrm{d}\lambda_e}{\mathrm{d}\nu} = -\frac{\partial\mathcal{H}}{\partial e} \quad , \quad \frac{\mathrm{d}\lambda_\omega}{\mathrm{d}\nu} = -\frac{\partial\mathcal{H}}{\partial \omega} \quad , \quad \frac{\mathrm{d}\lambda_t}{\mathrm{d}\nu} = -\frac{\partial\mathcal{H}}{\partial t} \quad , \quad \frac{\mathrm{d}\lambda_{ap}}{\mathrm{d}\nu} = -\frac{\partial\mathcal{H}}{\partial a_{p_{\min}}} \tag{18}$$

whose full expressions, obtained with a symbolic manipulation software, are here omitted for the sake of brevity. From the Pontryagin's maximum principle, the optimal control law $\tau = \tau(\nu)$ is such that, at any value of true anomaly ν, the Hamiltonian function is an absolute maximum. In particular, since $\mathcal{H}$ is a linear function of τ, see Eqs. (10)–(11) and (16), the optimal solution is a bang-bang control [25], viz.

$$\tau = \frac{\mathrm{sign}\,(S_W)+1}{2} \qquad \text{with} \qquad S_W \triangleq \frac{\partial\mathcal{H}}{\partial\tau} \tag{19}$$

where $\mathrm{sign}\,(\cdot)$ is the signum function, while S_W is obtained from Eq. (17). Finally, the transversality condition [24] gives three additional boundary conditions

$$\lambda_{ap}(\nu_0) = 1 \quad , \quad \lambda_{ap}(\nu_f) = -1 \quad , \quad \lambda_t(\nu_f) = -\Omega_\oplus\,\lambda_\omega(\nu_f) \tag{20}$$

The resulting two-point boundary value problem (TPBVP) is therefore described by the 10 differential equations (1)–(4), (15), and (18), with the 10 boundary constraints (12), (14), and (20). The TPBVP has been solved using the procedure described in Ref. [26], while the differential equations have been numerically integrated in double precision using a variable order Adams-Bashforth-Moulton solver scheme [27, 28] with absolute and relative errors of 10^{-12}.

2.3. Necessary propulsive level

The optimal control problem described in the last section has been solved, parametrically, as a function of the design parameter $n \in [1,\, 2]$; see also Eq. (9). The numerical results, obtained by solving about 30 optimal control problems, are collected in Fig. 5, where the function $a_{p_{\min}}^{(\min)} = a_{p_{\min}}^{(\min)}(n)$ describes how the required (minimum) propulsive acceleration magnitude varies with n.

The curve $a_{p_{\min}}^{(\min)} = a_{p_{\min}}^{(\min)}(n)$ is close to a hyperbola, whose analytic expression is

$$a_{p_{\min}}^{(\min)} \simeq \frac{a_{p_{\min}}^\star}{n} \qquad \text{with} \qquad a_{p_{\min}}^\star \triangleq 0.0974\,\mathrm{mm/s^2} \tag{21}$$

where $a_{p_{\min}}^\star$ is the value of $a_{p_{\min}}^{(\min)}$ when $n = 1$; see Fig. 5. This interesting result is in agreement with the numerical simulations which show that, for each value of $n \in [1,\, 2]$, the optimal control law is $\tau(\nu) = 1$, that is, the ECS is switched on along the whole SPSD revolution. Therefore, the SPSD acts like a Sun-pointing millimeter-scale solar sail (without ECS) in which the thermo-optical characteristics of the reflective film are constant, and the degradation effects [29, 30, 31, 22] are neglected. This behavior is by no means surprising, since the condition $\tau(\nu) \equiv 1$ allows the SPSD to exploit, at each time, the maximum propulsive acceleration magnitude $a_{p_{\max}} = n\,a_{p_{\min}}$ and, therefore, to minimize $a_{p_{\min}}$ for a given value of n.

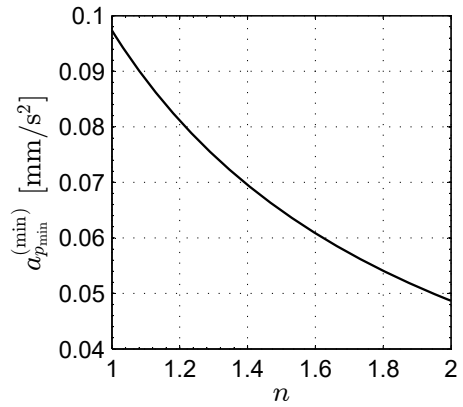

Figure 5: Minimum value of $a_{p_{\min}}$ as a function of n, when $a_0 = 17\,R_\oplus$ and $e_0 = 12/34$.

Conversely, the maximum value of $a_{p_{\min}}$, that is, the upper limit of the minimum propulsive acceleration magnitude necessary for the apse line to precess, is obtained when the ECS is switched off along the entire SPSD revolution, viz. $\tau(\nu) \equiv 0$. This intuitive result is confirmed by a more rigorous analysis in which the control law $\tau = \tau(\nu)$ is chosen such as to minimize (instead of maximizing) the performance index J given by Eq. (13). In this case, Eq. (19) is replaced by

$$\tau = \frac{1 - \text{sign}\,(S_W)}{2} \qquad \text{with} \qquad S_W \triangleq \frac{\partial \mathcal{H}}{\partial \tau} \tag{22}$$

whose solution gives the optimal control law which minimizes, at any value of ν, the Hamiltonian function defined in Eq. (16). In this case, for each $n \in [1, 2]$, the maximum admissible value of the minimum propulsive acceleration magnitude is constant with $a_{p_{\min}}^{(\max)} \triangleq \max\{a_{p_{\min}}\} = a_{p_{\min}}^\star$. In other terms, for a given value of n, the value of $a_{p_{\min}}$ is to be chosen in the range

$$a_{p_{\min}} \in \left[\frac{a_{p_{\min}}^\star}{n},\, a_{p_{\min}}^\star \right] \tag{23}$$

or, equivalently, the pair $\{n,\, a_{p_{\min}}\}$ must be selected in the admissible region $\mathcal{S}$ defined in Fig. 6. In particular, the boundary of the admissible region $\mathcal{S}$ is determined by the two functions $a_{p_{\min}}^{(\min)} = a_{p_{\min}}^{(\min)}(n)$ and $a_{p_{\min}}^{(\max)} = a_{p_{\min}}^{(\max)}(n)$, and gives all of the pairs $\{n,\, a_{p_{\min}}\}$ for which the ECS is always switched on or off, respectively.

When, instead, a generic pair $\{n,\, a_{p_{\min}}\}$ coincides with a point inside the admissible region $\mathcal{S}$, the optimal control law contains both arcs with $\tau = 0$ and arcs with $\tau = 1$. In particular, when the value of n and $a_{p_{\min}}$ is fixed, according to the approach of Ref. [7] the ν-variation of the switching parameter τ can be obtained by minimizing the control effort required to achieve the desired (artificial) apse-line precession. Accordingly, for a given pair $\{n,\, a_{p_{\min}}\} \in \mathcal{S}$ the function $\tau = \tau(\nu)$ is chosen such as to maximize the performance index $J_{ac} \leq 0$ defined as

$$J_{ac} \triangleq -\int_0^{2\pi} \tau \,\mathrm{d}\nu \tag{24}$$

where the subscript ac is used to emphasize that the minimum propulsive acceleration is constrained equal to $a_{p_{\min}}$. Note that, in the limit case of $\max[J_{ac}] = 0$ (or $\max[J_{ac}] = -2\pi$), the ECS is switched off (or switched on) along the whole SPSD revolution, i.e. $\tau = 0$ (or $\tau = 1$) for $\nu \in [0,\, 2\pi]$ rad. From Eq. (24), the Hamiltonian function now becomes [24]

$$\mathcal{H}_{ac} \triangleq \mathcal{H} - \tau \tag{25}$$

where $\mathcal{H}$ is given by Eq. (16). The Euler-Lagrange equations are still given by Eqs. (18), whereas the optimal control law is

$$\tau = \frac{\text{sign}\,(S_{W_{ac}}) + 1}{2} \qquad \text{with} \qquad S_{W_{ac}} \triangleq \frac{\partial \mathcal{H}_{ac}}{\partial \tau} = \frac{\partial \mathcal{H}}{\partial \tau} - 1 \equiv S_W - 1 \tag{26}$$

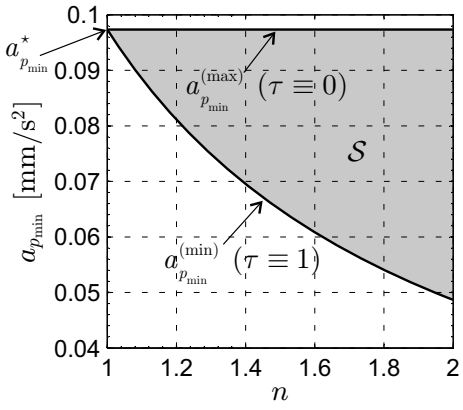

Figure 6: Admissible region $\mathcal{S}$ when $a_0 = 17\,R_\oplus$ and $e_0 = 12/34$.

where S_W is defined in Eq. (19). A potential mission scenario that involves a low-performance SPSD, where the optimal control law is given by Eq. (26), is discussed in the next section.

2.4. Case study

Consider the low-performance SPSD_1 with $n = 1.8$ and $a_{p_{\min}} = 0.0794\,\text{mm/s}^2$; see Tab. 1. The pair $\{n,\, a_{p_{\min}}\}$ associated with the SPSD_1 corresponds to a point inside the admissible region $\mathcal{S}$ defined in Fig. 6. In this case, the optimal control law that guarantees the desired artificial precession of the apse line, obtained through Eq. (26), is given by

$$\tau(\nu) = \begin{cases} 0 & \text{if} \quad \nu \in [0,\, 119.6)\,\text{deg} \\ 1 & \text{if} \quad \nu \in [119.6,\, 151.6)\,\text{deg} \\ 0 & \text{if} \quad \nu \in [151.6,\, 208.4)\,\text{deg} \\ 1 & \text{if} \quad \nu \in [208.4,\, 240.4)\,\text{deg} \\ 0 & \text{if} \quad \nu \in [240.4,\, 360]\,\text{deg} \end{cases} \tag{27}$$

The function $\tau = \tau(\nu)$ is nearly symmetric with respect to the apse line, and has two arcs in which the ECS is switched on; see also Fig. 7.

Figure 8 shows the ν-variation of both the smart dust osculating orbital elements $\{a,\, e,\, \omega\}$, and the angle δ which localizes the direction of the Earth-Sun line; see also Fig. 2. In particular, ω closely follows the value of δ, while it is exactly equal to δ when $\nu = \{0,\, 2\,\pi\}\,\text{rad}$, in agreement with the constraints of Eqs. (12) and (14) [recall Eq. (8)]. This interesting behavior is illustrated in Fig. 9, which draws the difference $(\omega - \delta)$ between the orientation of the osculating orbit apse line and the Earth-Sun direction. The maximum value of $|\omega - \delta|$ is less than $0.25\,\text{deg}$, that is, the osculating orbit apse line is nearly aligned with the Earth-Sun direction at any time (or at any value of ν).

Finally, Fig. 8 shows that $a/a_0 \simeq 1$ and $e/e_0 \simeq 1$, that is, the value of the osculating orbit semimajor axis and eccentricity are close to their design orbital values a_0 and e_0, respectively. This point is at the heart of the analytical approximation of the admissible region $\mathcal{S}$ discussed in the next section. Note that the behavior of $a = a(\nu)$ and $e = e(\nu)$ shown in Fig. 8 is representative of a generic mission scenario in which the pair $\{n,\, a_{p_{\min}}\}$ is selected in the admissible region $\mathcal{S}$ defined in Fig. 6.

3. Analytical approximation of the admissible region

According to the typical behavior of the state variables illustrated in Fig. 8, the simplification is now made that both the osculating orbit semimajor axis and eccentricity do not vary with time, and the apse

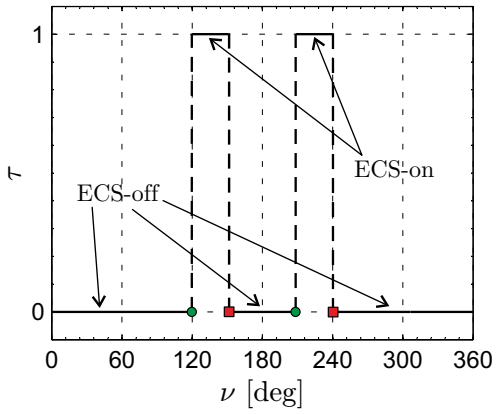

(a) ν-variation of τ.

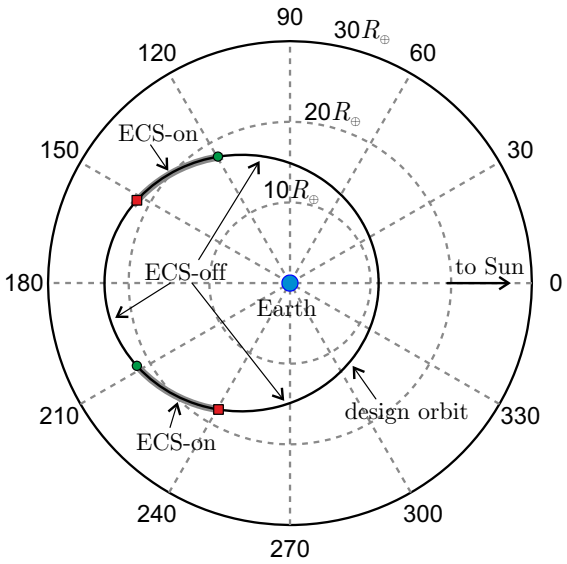

(b) ECS switching strategy.

Figure 7: Optimal control law for the SPSD_1, when $a_0 = 17\,R_\oplus$ and $e_0 = 12/34$.

line is always aligned with the Earth-Sun direction. In other terms, it is assumed that $a = a_0$, $e = e_0$, and $\delta = \omega$ for $\nu \in [0,\, 2\,\pi]$ rad. Bearing in mind Eq. (8), Eqs. (10)–(11) become

$$a_{p_r} = -a_{p_{\min}}\,\left[1 + \tau\,(n-1)\right]\,\cos\left(\nu\right) \tag{28}$$

$$a_{p_t} = a_{p_{\min}}\,\left[1 + \tau\,(n-1)\right]\,\sin\left(\nu\right) \tag{29}$$

so that, with the aid of the second of Eqs. (5), Eq. (3) reduces to the compact expression

$$\frac{\mathrm{d}\omega}{\mathrm{d}\nu} = a_{p_{\min}}\,\left[1 + \tau\,(n-1)\right]\,\left(\frac{a_0^2}{\mu_\oplus}\right)\,f(e_0,\,\nu) \tag{30}$$

where $f = f(e_0,\,\nu)$ is a dimensionless auxiliary function defined as

$$f(e_0,\,\nu) \triangleq \frac{\left(2 - \cos^2\nu + e_0\,\cos\nu\right)\,\left(1 - e_0^2\right)^2}{e_0\,\left(1 + e_0\,\cos\nu\right)^3} \tag{31}$$

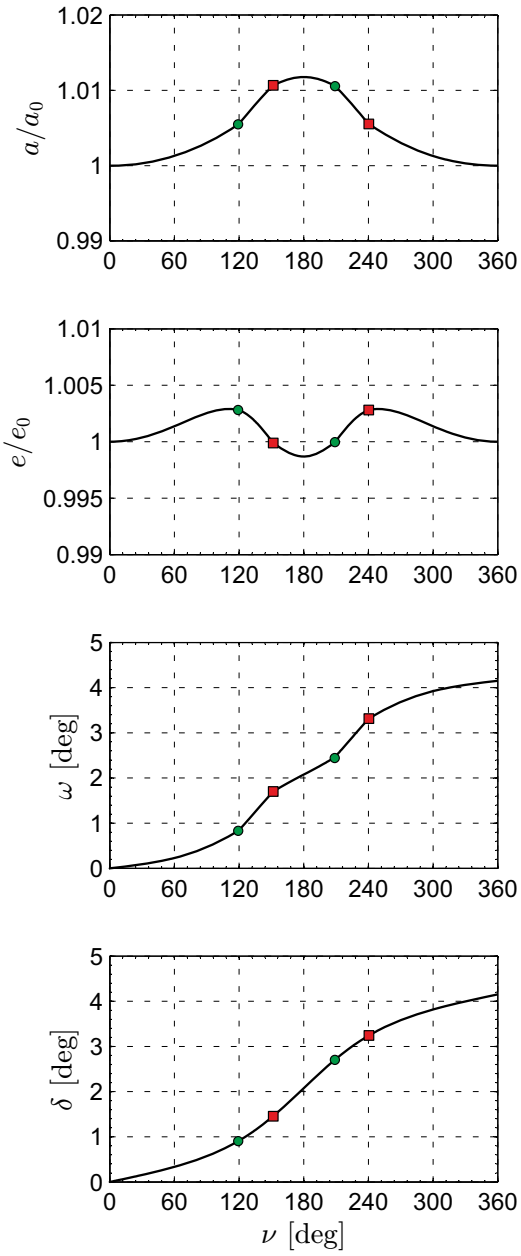

Figure 8: Variation with ν of the osculating orbit elements for the SPSD$_1$, when $a_0 = 17\,R_\oplus$ and $e_0 = 12/34$. Green circles: ECS-on; red squares: ECS-off.

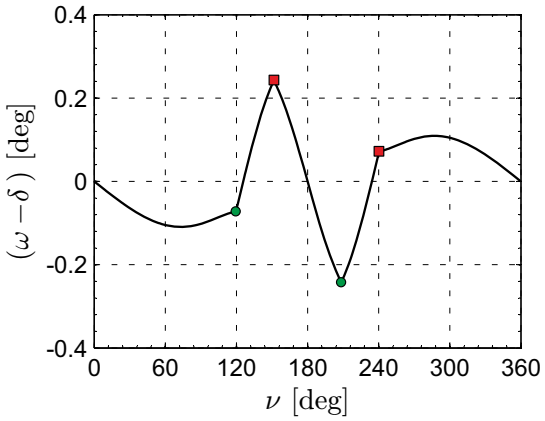

Figure 9: Angle $(\omega - \delta)$ between the apse line and the Earth-Sun direction, when $a_0 = 17\,R_\oplus$ and $e_0 = 12/34$.

When the switching parameter takes a constant value for $\nu \in [0,\, 2\pi]$ rad, that is, when either $\tau \equiv 0$ or $\tau \equiv 1$ along the whole SPSD revolution around the Earth, Eq. (30) may be used to get an analitycal/graphical relation between the propulsive requirements (in terms of $a_{p_{\min}}$ and n) and the characteristics of the design orbit $\{a_0,\, e_0\}$.

3.1. Case of $\tau \equiv 0$ during the SPSD revolution

Assume the ECS to be switched off during the whole revolution around the Earth, that is, $\tau \equiv 0$. In this case, Eq. (30) reduces to

$$\frac{\mathrm{d}\omega}{\mathrm{d}\nu} = a_{p_{\min}}^{(\max)} \left(\frac{a_0^2}{\mu_\oplus}\right) f(e_0,\, \nu) \tag{32}$$

which, by separation of variables, gives the variation of the argument of perigee $\Delta\omega \triangleq \omega(\nu_f) - \omega(\nu_0) \equiv \omega(\nu_f)$ in a single SPSD revolution, viz.

$$\omega(\nu_f) = a_{p_{\min}}^{(\max)} \left(\frac{a_0^2}{\mu_\oplus}\right) F \tag{33}$$

where the dimensionless quantity $F = F(e_0)$ depends on the design orbit eccentricity e_0 as

$$F = \int_0^{2\pi} f(e_0,\, \nu)\, \mathrm{d}\nu \equiv \frac{\left(1 - e_0^2\right)^2\, G}{e_0} \tag{34}$$

with

$$G = G(e_0) \triangleq \int_0^{2\pi} \frac{2 - \cos^2\nu + e_0\, \cos\nu}{\left(1 + e_0\, \cos\nu\right)^3}\, \mathrm{d}\nu \tag{35}$$

The integral in the right hand side of Eq. (35) can be solved parametrically (as a function of e_0) with standard numerical methods, such as the adaptive recursive Simpson's rule [32], which is implemented in the MATLAB built-in function "`quad`". The function $G = G(e_0)$ is reported in Fig. 10 when $e_0 \in [0,\, 0.9]$. Using a curve fitting procedure, the function $G = G(e_0)$ can be approximated, with an absolute error less than 0.1, by the equation

$$G(e_0) \simeq \frac{7.003}{e_0^4 - 1.189\, e_0^3 - 0.4256\, e_0^2 - 0.1484\, e_0 + 0.7508} \tag{36}$$

At the end of the revolution around the Earth, when the flight time t_f is close to the Keplerian orbital period of the design orbit, that is

$$t_f = 2\,\pi \sqrt{\frac{a_0^3}{\mu_\oplus}} \tag{37}$$

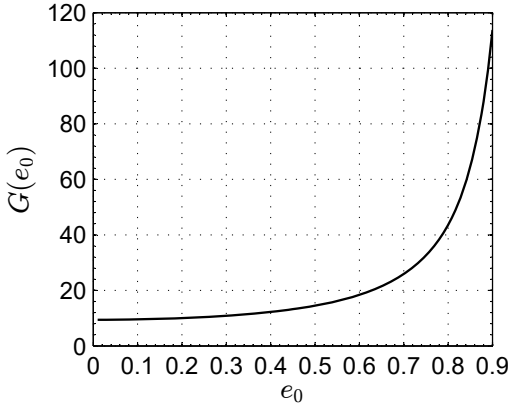

Figure 10: Auxiliary function $G = G(e_0)$, see Eq. (35).

the angle δ between the reference (fixed) direction and the Earth-Sun line is [see Eq. (8)]

$$\delta(\nu_f) \equiv \delta(t_f) = 2\,\pi\,\Omega_\oplus \sqrt{\frac{a_0^3}{\mu_\oplus}} \tag{38}$$

Enforcing the condition for which the SPSD apse line is aligned with the Earth-Sun line at the end of the orbital period, that is, $\omega(\nu_f) = \delta(\nu_f)$, from Eqs. (33) and (38) the analytical expression of $a_{p_{\min}}^{(\max)}$ is obtained as

$$a_{p_{\min}}^{(\max)} = \frac{2\,\pi\,\Omega_\oplus\,e_0}{G\,\left(1-e_0^2\right)^2}\sqrt{\frac{\mu_\oplus}{a_0}} \tag{39}$$

where G is given by either Eq. (36) or Fig. 10 as a function of e_0. For example, when $a_0 = 17\,R_\oplus$ and $e_0 = 12/34$, Eq. (39) gives $a_{p_{\min}}^{(\max)} \simeq 0.096\,\mathrm{mm/s^2}$, a value very close to the actual (numerical) result $a_{p_{\min}}^{\star} \simeq 0.0974\,\mathrm{mm/s^2}$; see also Fig. 6.

Notably, in the special case when $e_0 = 0$, Eq. (39) states that $a_{p_{\min}}^{(\max)} = 0$, that is, the design orbit apse line precesses without any propulsive acceleration. This seemingly odd result can be explained by the fact that a circular design orbit ($e_0 = 0$), may be thought of as the limiting case when the number of apse lines tends to infinity and, therefore, the Earth-Sun direction is always aligned with one of these lines.

3.2. Case of $\tau \equiv 1$ during the SPSD revolution

Assume now that the ECS is always switched on during the SPSD revolution around the Earth, that is, $\tau \equiv 1$. In this case, Eq. (30) gives

$$\frac{\mathrm{d}\omega}{\mathrm{d}\nu} = n\,a_{p_{\min}}^{(\min)}\left(\frac{a_0^2}{\mu_\oplus}\right)\,f(e_0,\,\nu) \tag{40}$$

which coincides with Eq. (32) when $a_{p_{\min}}^{(\max)}$ is formally replaced by $n\,a_{p_{\min}}^{(\min)}$. As such, paralleling the procedure discussed in the last section, the analytical approximation of the minimum value of $a_{p_{\min}}$ is

$$a_{p_{\min}}^{(\min)} = \frac{a_{p_{\min}}^{(\max)}}{n} \equiv \frac{2\,\pi\,\Omega_\oplus\,e_0}{n\,G\,\left(1-e_0^2\right)^2}\sqrt{\frac{\mu_\oplus}{a_0}} \tag{41}$$

where G is again given by Eq. (36) or Fig. 10. Note that $a_{p_{\min}}^{(\min)}$ varies as $1/n$, according to the curve in Fig. 5 and the approximate relationship of Eq. (21).

Equations (39) and (41) can be used to perform a parametric analysis of the SPSD propulsive requirements as a function of the design orbit characteristics $\{a_0,\,e_0\}$, as is discussed in the next section.

3.3. Parametric analysis of propulsive requirements

Consider a SPSD orbit with a perigee radius $r_p = 11\,R_\oplus$ and an apogee radius ranging in the interval $r_a \in [22,\, 30]\,R_\oplus$. Such a variation of r_a is consistent with a possible *in-situ* exploration of the downstream region of Earth's magnetosphere [2]. When r_a is taken as a free parameter, the admissible ranges of variation for a_0 and e_0 are

$$a_0 = a_0(r_a) = \frac{r_p + r_a}{2} \in [16.5,\, 20.5]\,R_\oplus \qquad , \qquad e_0 = e_0(r_a) = \frac{r_a - r_p}{r_a + r_p} \in [1/3,\, 19/41] \tag{42}$$

Accordingly, the values of $a_{p_{\min}}^{(\min)}$ and $a_{p_{\min}}^{(\max)}$ are estimated, as functions of r_a, by substituting Eqs. (42) into Eqs. (39) and (41). The result corresponding to $n = 1.8$ is shown in Fig. 11. In particular, the value of $a_{p_{\min}}^{(\min)}$ increases of about 26% when the apogee radius varies from its design value of $23\,R_\oplus$ to the upper limit of $30\,R_\oplus$.

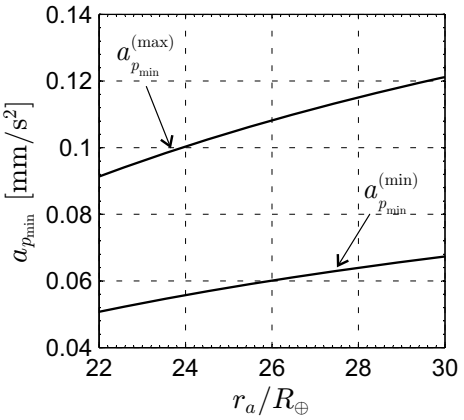

Figure 11: Propulsive requirements as a function of the design orbit apogee radius r_a, with $r_p = 11\,R_\oplus$ and $n = 1.8$.

On the other hand, a greater value of r_a (and, therefore, a more elliptical working orbit) implies a longer length of time in the downstream region of Earth's magnetosphere. For exemplary purposes, assume that the scientific phase of the mission (that is, the *in-situ* analysis of the magnetotail) starts when the Earth-SPSD distance is $r > r^\star \triangleq 15 R_\oplus$. The length of the scientific phase $\Delta t_{\rm sp}$ for each orbit can be calculated, as a function of r_a, by solving a Kepler's problem [33], and the result is

$$\Delta t_{\rm sp} = \frac{2\,\pi - 2\,\left(E^\star - e_0\,\sin E^\star\right)}{\sqrt{\mu_\oplus / a_0^3}} \tag{43}$$

where $E^\star$ is the eccentric anomaly at $r = r^\star$, given by

$$E^\star = 2\,\arctan\left[\sqrt{\frac{1-e_0}{1+e_0}}\,\tan\left(\frac{\nu^\star}{2}\right)\right] \tag{44}$$

in which

$$\nu^\star = \arccos\left[\frac{a_0\,\left(1-e_0^2\right) - r^\star}{e_0\,r^\star}\right] \tag{45}$$

Recalling Eqs. (42), the function $\Delta t_{\rm sp} = \Delta t_{\rm sp}(r_a)$ of Eq. (43) is drawn in Fig. 12.

Combining the information given by Figs. 11 and 12, and using the length of time of the scientific phase as a free parameter, $a_{p_{\min}}^{(\min)}$ and $a_{p_{\min}}^{(\max)}$ are reported in Fig. 13 as a function of $\Delta t_{\rm sp}$. The figure clearly shows that a tradeoff between the propulsive requirements (in terms of $a_{p_{\min}}^{(\min)}$) and $\Delta t_{\rm sp}$ is easily obtained from Eqs. (39), (41) and (43).

Notably, Eq. (39) can also be applied when a conventional Sun-pointing solar sail is used to artificially precess the orbit's apse line. In that case, the solar sail attitude may be passively maintained using a

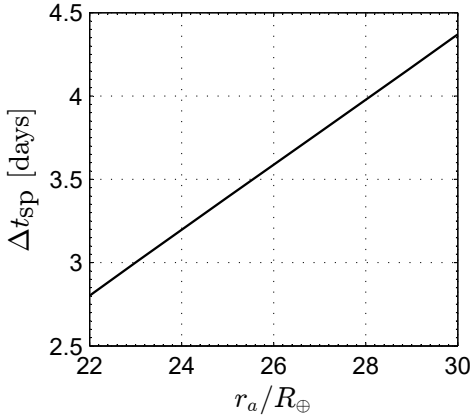

Figure 12: Length of the scientific phase for each orbit as a function of the apogee radius, when $r_p = 11R_\oplus$ and $r^\star = 15R_\oplus$.

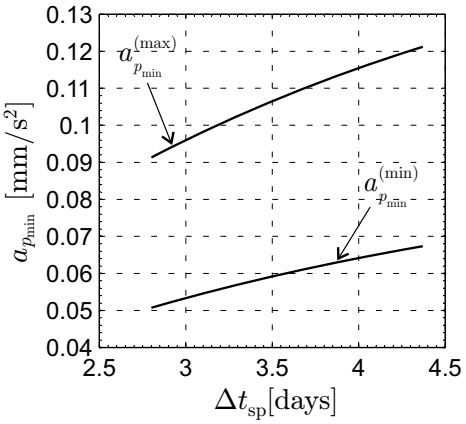

Figure 13: Propulsive requirements as a function of $\Delta t_{\rm sp}$, when $r_p = 11\,R_\oplus$, $r^\star = 15R_\oplus$ and $n = 1.8$.

conically shaped structure, and Eq. (39) provides the characteristic acceleration necessary for achieving the desired precession. The solar sail film can be partially covered with electrochromic material panels [34], which allow the propulsive acceleration to be varied by switching them on (or off), in a similar way as that illustrated for a SPSD; see Fig. 14. The approximate model proposed in this work may be therefore applied in the same way to this more classical mission scenario.

4. Conclusions

This paper has discussed the application of a Sun-pointing smart dust to the GeoSail mission scenario, whose aim is the scientific exploration of the Earth's magnetic tail. The required working orbit is highly elliptical, and an artificial apse line precession must be induced, in order to constantly align the orbital apse-line with the Sun-Earth direction. Assuming that the smart dust is equipped with an electrochromic-based control system capable of modifying the propulsive acceleration magnitude generated by the solar radiation pressure, an optimal control problem has been solved to identify the performance requirements of the proposed mission scenario.

Since the semimajor axis and the eccentricity of the osculating orbit have negligible variations during the artificially-induced precession, an approximate mathematical model has been derived and discussed, based on the assumption that these parameters remain constant along the whole revolution around the Earth. Once the desired length of time in the magnetotail region is chosen, the semi-analytical results of

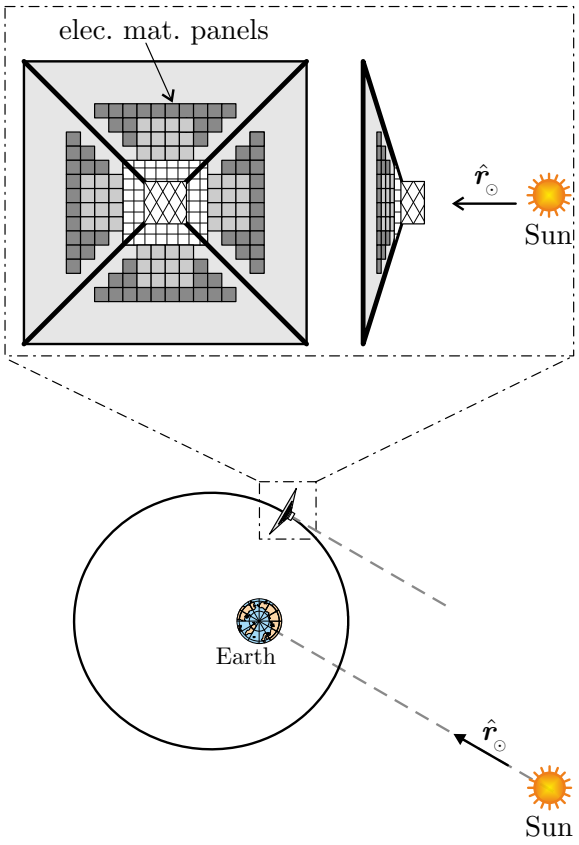

Figure 14: Sun-pointing solar sail-based concept, with electrochromic material panels, for geomagnetic tail exploration.

the approximate model offer a simple means to calculate the propulsive requirements of the smart dust in terms of acceleration magnitude. The simulation results show that this concept is feasible with current or near-term technological level.

Acknowledgements

This work is supported by the University of Pisa, Progetti di Ricerca di Ateneo (Grant no. PRA_2018_44).

References

[1] M. Galland Kivelson, F. Bagenal, Encyclopedia of the Solar System, 3rd Edition, Elsevier , 2014, Ch. 7, pp. 137–157.
[2] M. Macdonald, C. R. McInnes, D. Alexander, A. Sandman, GeoSail: Exploring the magnetosphere using a low-cost solar sail, Acta Astronautica 59 (8-11) (2006) 757–767, doi: 10.1016/j.actaastro.2005.07.023.
[3] C. R. McInnes, M. Macdonald, V. Angelopolous, D. Alexander, GEOSAIL: Exploring the geomagnetic tail using a small solar sail, Journal of Spacecraft and Rockets 38 (4) (2001) 622–629, doi: 10.2514/2.3727.
[4] P. Falkner, Executive summary of the GeoSail study, Technology Reference Study SCI-A/2006/005/GS, European Space Agency, Science Payload and Advanced Concept Office (2007).
URL `http://sci.esa.int/trs/38980-geosail/`
[5] V. Lappas, G. Mengali, A. A. Quarta, J. Gil-Fernandez, T. Schmidt, B. Wie, Practical systems design for an earth-magnetotail-monitoring solar sail mission, Journal of Spacecraft and Rockets 46 (2) (2009) 381–393, doi: 10.2514/1.32040.
[6] J. L. Wright, Space Sailing, Gordon and Breach Science Publishers , 1992, pp. 223–233.
[7] G. Mengali, A. A. Quarta, V. J. Lappas, Optimal steering law for the GeoSail mission, Journal of Guidance, Control, and Dynamics 30 (3) (2007) 876–879, doi: 10.2514/1.28765.
[8] C. Colombo, C. R. McInnes, Orbital dynamics of "smart-dust" devices with solar radiation pressure and drag, Journal of Guidance, Control, and Dynamics 34 (6) (2011) 1613–1631, doi: 10.2514/1.52140.

[9] C. Colombo, C. Lücking, C. R. McInnes, Orbital dynamics of high area-to-mass ratio spacespace with J_2 and solar radiation pressure for novel earth observation and communication services, Acta Astronautica 81 (1) (2012) 137–150, doi: 10.1016/j.actaastro.2012.07.009.
[10] C. Colombo, C. R. McInnes, Orbit design for future spacechip swarm missions in a planetary atmosphere, Acta Astronautica 75 (2012) 25–41, doi: 10.1016/j.actaastro.2012.01.004.
[11] C. Colombo, C. Lücking, C. R. McInnes, Orbit evolution, maintenance and disposal of spacechip swarms through electrochromic control, Acta Astronautica 82 (1) (2013) 25–37, doi: 10.1016/j.actaastro.2012.05.035.
[12] J. A. Atchison, M. A. Peck, A passive, sun-pointing, millimeter-scale solar sail, Acta Astronautica 67 (1–2) (2010) 108–121, doi: 10.1016/j.actaastro.2009.12.008.
[13] L. Niccolai, M. Bassetto, A. A. Quarta, G. Mengali, Solar sailing with femtosatellites: a review of smart dust architecture, dynamics, and mission applications, Submitted. Progress in Aerospace Sciences .
[14] C. Lücking, C. Colombo, C. R. McInnes, Orbit control of high area-to-mass ratio spacecraft using electrochromic coating, in: 61st International Astronautical Congress (IAC), Prague, Czech Republic, 2010, pp. 1923–1937.
[15] C. Lücking, C. Colombo, C. R. McInnes, Electrochromic orbit control for smart-dust devices, Journal of Guidance, Control, and Dynamics 35 (5) (2012) 1548–1558, doi: 10.2514/1.55488.
[16] Z. Manchester, M. A. Peck, A. Filo, KickSat: A crowd-funded mission to demonstrate the world's smallest spacecraft, in: 27th Annual AIAA/USU Conference on Small Satellites, Logan, UT, USA, 2013.
[17] J. P. W. Stark, G. G. Swinerd, P. W. Fortescue, Spacecraft Systems Engineering, 3rd Edition, Wiley, 2003, Ch. 4, pp. 93–95.
[18] G. Mengali, A. A. Quarta, Heliocentric trajectory analysis of sun-pointing smart dust with electrochromic control, Advances in Space Research 57 (4) (2016) 991–1001, doi: 10.1016/j.asr.2015.12.017.
[19] A. A. Quarta, G. Mengali, E. Denti, Optimal in-orbit repositioning of sun-pointing smart dust, Acta Astronautica 154 (2019) 278–285, doi: 10.1016/j.actaastro.2018.03.036.
[20] G. Mengali, A. A. Quarta, E. Denti, Relative motion of sun-pointing smart dust in circular heliocentric orbits, Journal of Guidance, Control and Dynamics 41 (4) (2018) 1009–1014, doi: 10.2514/1.G003088.
[21] C. R. McInnes, Solar Sailing: Technology, Dynamics and Mission Applications, Springer-Verlag Berlin , 1999, Ch. 2, pp. 46–51.
[22] G. Mengali, A. A. Quarta, C. Circi, B. Dachwald, Refined solar sail force model with mission application, Journal of Guidance, Control, and Dynamics 30 (2) (2007) 512–520, doi: 10.2514/1.24779.
[23] D. Alexander, C. R. McInnes, V. Angelopoulos, A. W. Sandman, M. Macdonald, Geosail: A novel solar sail mission concept for geospace, AIP Conference Proceedings 608 (2002) 305–312, doi: 10.1063/1.1449739.
[24] A. E. Bryson, Y. C. Ho, Applied Optimal Control, Hemisphere Publishing Corporation , New York, NY, 1975, Ch. 2, pp. 71–89, ISBN: 0-891-16228-3.
[25] R. F. Stengel, Optimal Control and Estimation, Dover Publications, inc. , 1994, pp. 222–254.
[26] A. A. Quarta, G. Mengali, A. Caruso, Optimal circle-to-rectilinear orbit transfer with circumferential thrust, Astrodynamics 3 (1) (2019) 31–43, doi: 10.1007/s42064-018-0034-9.
[27] L. F. Shampine, M. K. Gordon, Computer Solution of Ordinary Differential Equations: The Initial Value Problem, W. H. Freeman , San Francisco, 1975, Ch. 10.
[28] L. F. Shampine, M. W. Reichelt, The MATLAB ODE suite, SIAM Journal on Scientific Computing 18 (1) (1997) 1–22, doi: 10.1137/S1064827594276424.
[29] B. Dachwald, W. Seboldt, M. Macdonald, G. Mengali, A. A. Quarta, C. R. McInnes, L. Rios-Reyes, D. J. Scheeres, B. Wie, M. Görlich, F. Lura, B. Diedrich, V. Baturkin, V. L. Coverstone, M. Leipold, G. P. Garbe, Potential solar sail degradation effects on trajectory and attitude control, in: AIAA Guidance, Navigation, and Control Conference and Exhibit, San Francisco, USA, 2005, paper AIAA 2005-6172.
[30] B. Dachwald, G. Mengali, A. A. Quarta, M. Macdonald, Parametric model and optimal control of solar sails with optical degradation, Journal of Guidance, Control, and Dynamics 29 (5) (2006) 1170–1178, doi: 10.2514/1.20313.
[31] B. Dachwald, M. Macdonald, C. R. McInnes, G. Mengali, A. A. Quarta, Impact of optical degradation on solar sail mission performance, Journal of Spacecraft and Rockets 44 (4) (2007) 740–749, doi: 10.2514/1.21432.
[32] J. H. Mathews, K. D. Fink (Eds.), Numerical Methods: Using MATLAB, 4th Edition, Pearson Prentice Hall , Upper Saddle River, New Jersey, 2004, Ch. 7, pp. 392–399.
[33] J. E. Prussing, B. A. Conway, Orbital Mechanics, Oxford University Press , New York, 1993, Ch. 2, pp. 26–32.
[34] G. Aliasi, G. Mengali, A. A. Quarta, Artificial lagrange points for solar sail with electrochromic material panels, Journal of Guidance, Control, and Dynamics 36 (5) (2013) 1544–1550, doi: 10.2514/1.58167.